Ab Initio Treatment of the Chemical Reaction Precursor Complex Br(2P)−HCN. 2. Bound-State Calculations and Infrared Spectra[†]

Anna V. Fishchuk,[§] Jeremy M. Merritt,[‡,||] Gerrit C. Groenenboom,[§] and Ad van der Avoird*,[§]

Theoretical Chemistry, IMM, Radboud University Nijmegen, Toernooiveld 1, 6525 ED Nijmegen, The Netherlands, and Department of Chemistry, University of North Carolina, Chapel Hill, North Carolina 27599

Rovibronic energy levels and properties of the Br(2P)−HCN complex were obtained from three-dimensional calculations, with HCN kept linear and the CN bond frozen. All diabatic states that correlate to the $^2P_{3/2}$ and $^2P_{1/2}$ states of the Br atom were included and spin−orbit coupling was taken into account. The 3×3 matrix of diabatic potential surfaces was taken from the preceding paper (paper 1). In agreement with experiment, we found two linear isomers, Br−NCH and Br−HCN. The calculated binding energies are very similar: D_0 = 352.4 cm^{-1} and D_0 = 349.1 cm^{-1}, respectively. We established, also in agreement with experiment, that the ground electronic state of Br−NCH has $|\Omega| = (^1/_2)$ and that Br−HCN has a ground state with $|\Omega| = (^3/_2)$, where the quantum number, Ω, is the projection of the total angular momentum, J, of the complex on the intermolecular axis R. This picture can be understood as being caused by the electrostatic interaction between the quadrupole of the Br(2P) atom and the dipole of HCN, combined with the very strong spin−orbit coupling in Br. We predicted the frequencies of the van der Waals modes of both isomers and found a direct Renner−Teller splitting of the bend mode in Br−HCN and a smaller, indirect, splitting in Br−NCH. The red shift of the CH stretch frequency in the complex, relative to free HCN, was calculated to be 1.98 cm^{-1} for Br−NCH and 23.11 cm^{-1} for Br−HCN, in good agreement with the values measured in helium nanodroplets. Finally, with the use of the same potential surfaces, we modeled the Cl(2P)−HCN complex and found that the experimentally observed linear Cl−NCH isomer is considerably more stable than the (not observed) Cl−HCN isomer. This was explained mainly as an effect of the substantially smaller spin−orbit coupling in Cl, relative to Br.

1. Introduction

The series of weakly bound complexes X−HY has received an increasing amount of attention, both experimental[1−5] and theoretical,[6−13] especially in view of their role as reaction precursors in the hydrogen exchange reactions X + HY → HX + Y, with X, Y = F, Cl, Br, O, OH, CN. Because of the open-shell configuration of the X radical in its ground state, electronic degeneracies occur in these complexes, and their theoretical description has to go beyond the Born−Oppenheimer approximation. One of the complexes recently studied experimentally by Merritt et al.[5] is Br(2P)−HCN. It was prepared in liquid helium nanodroplets in a molecular beam setup and studied by high-resolution infrared spectroscopy. This species is particularly interesting because it was found to occur in two isomeric forms: Br−HCN and Br−NCH, both linear. In the preceding paper, paper 1, we outlined a diabatic model that involves the asymptotically degenerate electronic states and their coupling, which is suitable to compute the rovibronic levels of this open-shell complex. We also presented ab initio calculated diabatic potential surfaces, both diagonal and off-diagonal, and

their analytic representation in a form that is convenient for bound-state calculations. The present paper describes the calculation of the rovibronic states and the comparison of the results with the experimental data.

2. Bound-State Calculations

The method that we apply to compute the rovibronic levels of Br(2P)−HCN is described in detail in ref 14 and has been used previously in our group to study Cl−HCl[10,11] and Cl−HF.[13] It is based on earlier work for open-shell atom closed-shell diatom complexes by Alexander[15] and by Dubernet and Hutson.[16,17] Of course, Br(2P)−HCN is not an atom−diatom complex, but for our goal the study of the structure and stability of this complex and its infrared spectrum associated with the CH stretch mode of HCN, it is justified to treat the HCN monomer as a pseudodiatom by fixing the CN bond length and keeping the molecule linear. More details on this approximation are given below.

The three internal coordinates varied are R, the length of the Jacobi vector **R** pointing from the Br nucleus to the center-of-mass of HCN, the CH bond length r_{CH}, and the angle θ between the vectors **R** and r_{CH}, where the latter is the vector pointing from the C nucleus to the H nucleus. The Hamiltonian is defined in a body-fixed(BF) frame with its z axis along **R** and r_{CH} in the xz plane

---

* Corresponding author. E-mail: A.vanderAvoird@theochem.ru.nl.
‡ Present address: Department of Chemistry, Emory University, Atlanta, Georgia 30322.
§ Radboud University Nijmegen.
|| University of North Carolina.

2. Bound-State Calculations and Infrared Spectra

J. Phys. Chem. A, Vol. 111, No. 31, 2007 **7271**

$$\hat{H} = \hat{H}_{HCN} + \frac{-\hbar^2}{2\mu_{AB}R} \frac{\partial^2}{\partial R^2} R +$$

$$\frac{|\hat{\mathbf{j}}_A + \hat{\mathbf{j}}_B|^2 - 2(\hat{\mathbf{j}}_A + \hat{\mathbf{j}}_B) \cdot \hat{\mathbf{J}} + \hat{\mathbf{J}}^2}{2\mu_{AB}R^2} +$$

$$A\hat{\boldsymbol{\lambda}} \cdot \hat{\mathbf{S}} + \sum_{\mu',\mu} |\lambda, \mu'\rangle V_{\mu',\mu}^{(\lambda)} (R, r_{CH}, \theta) \langle \lambda, \mu| \quad (1)$$

where μ_{AB} is the reduced mass of the atom (A = Br)-molecule (B = HCN) complex. The atomic masses are $m_H = 1.0078250321$ u, $m_C = 12$ u, $m_N = 14.0030740052$ u, and $m_{Br} = 78.9183376$ u. The operators $\hat{\boldsymbol{\lambda}}$ and $\hat{\mathbf{S}}$ and represent the orbital and spin angular momenta of the Br(^{2}P) atom, respectively, with the atomic quantum numbers $\lambda = 1$ and $S = (^1/_2)$. The operator $\hat{\mathbf{j}}_A = \hat{\boldsymbol{\lambda}} + \hat{\mathbf{S}}$ represents the total electronic angular momentum of the Br atom, whereas $\hat{\mathbf{j}}_B$ is the angular momentum associated with the rotation of the HCN monomer, and $\hat{\mathbf{J}}$ is the total angular momentum of the complex. We assume that the spin−orbit coupling in the Br atom is not affected by the relatively weak interaction with the HCN molecule so that we may use the atomic spin−orbit parameter $A = -2457$ cm^{-1} as a constant in eq 1. The 3×3 matrix of diabatic potentials $V_{\mu',\mu}^{(\lambda)}(R,r_{CH},\theta)$ that couple the diabatic states $|\lambda, \mu\rangle$ with projection $\mu = -1, 0, 1$ on the z axis was computed and described in paper 1.

The HCN monomer Hamiltonian is

$$\hat{H}_{HCN} = \frac{-\hbar^2}{2\mu_B r_{CH}} \frac{\partial^2}{\partial r_{CH}^2} r_{CH} + \frac{\hat{\mathbf{J}}_B^2}{2I(r_{CH})} + V_{HCN}(r_{CH}) \quad (2)$$

where $I(r_{CH})$ is the moment of inertia of linear HCN calculated as a function of the CH bond length with the CN bond fixed at the experimental equilibrium value $r_{CN} = 2.1793a_0$.[18] The reduced mass, μ_B, associated with the CH stretch coordinate, r_{CH}, is defined with the mass of the H atom and the mass $m_{CN} = m_C + m_N$ of the pseudoatom CN. The potential $V_{HCN}(r_{CH})$ was obtained from the accurate empirical HCN force field determined by Carter et al.[19] by keeping the molecule linear and fixing the CN bond length at $r_{CN} = 2.1793a_0$ (the same equilibrium value as used in the force field). In reality, the CH stretch mode of HCN also involves some stretching of the CN bond. The reason that we may consider the CN bond to be rigid in the present study is that we do not wish to determine the absolute frequency of the CH stretch mode in Br−HCN, but only the red shift of this mode caused by the interaction with the Br atom. The following arguments are used to justify our model. First, let us look at the results of ab initio calculations at the CCSD(T)/aug-cc-pVDZ level (for the acronyms, see paper 1). These results, displayed in Figure 1, show that the potential $V_{HCN}(r_{CH})$ computed with the CN bond frozen at its equilibrium distance practically coincides with the curve obtained by optimizing the CN distance for every value of r_{CH}. Second, in a normal-mode analysis with the force field of Carter et al.,[19] the amplitude of the CN stretch component involved in the harmonic normal coordinate of the CH stretch mode is quite small. Third, when we compute the CH stretch frequency with the full force field of Carter et al. and with the CN bond frozen, the values are 3310.81 and 3199.32 cm^{-1}, respectively. The harmonic values are 3414.27 and 3306.17 cm^{-1}. The experimental CH stretch frequency in HCN is 3310.81 cm^{-1}. Although the frequency changes considerably by fixing the CN bond length (the relative change is only 3% though), we believe that the model with CN frozen is sufficiently good to get a fairly

accurate red shift. In this context, it is also worthwhile to mention that there is a debate going on about whether the CN bond can be regarded as a spectator in the dynamics of different chemical reactions.[20−22]

The basis used to diagonalize the Hamiltonian of eq 1 is the same as that in ref 13. The radial basis $\chi_{n_R}(R)$ consists of a contracted set of sinc-DVR (sinc function discrete variable representation) functions. The contraction coefficients are the eigenvectors of a radial motion problem, solved by the sinc-DVR method[23] on a large grid, with the radial potential given by the isotropic component $v_{0,0}^0(R,r_{CH})$ of the diabatic Br−HCN potential $V_{0,0}(R,r_{CH},\theta)$, see eq 2 of paper 1, for $r_{CH} = 2.0440a_0$. This value of r_{CH} is one of the values on the grid described in paper 1; it is equal to the calculated equilibrium CH distance in HCN. To reach convergence of the radial basis more quickly, by including the effect of continuum wave functions, we added to this isotropic potential a term linear in R. The slope $\alpha = 219$ cm$^{-1}/a_0$ of this term was optimized variationally in calculations of the ground state and some low-lying levels of the complex. A similar basis $\phi_{n_r}(r_{CH})$ of contracted sinc-DVR functions was used for the CH stretch coordinate. The basis functions $\phi_{n_r}(r_{CH})$ are $j_B = 0$ eigenfunctions of the monomer Hamiltonian $\hat{H}_{HCN}$ in eq 2 computed by the sinc-DVR method. Here, it is not necessary to add a linear term because the potential $V_{HCN}(r_{CH})$ has a much deeper well than the intermolecular potential $V_{0,0}(R,r_{CH},\theta)$.

Because the spin−orbit coupling in the Br atom is very large, it is convenient for the interpretation of the results and the assignment of approximate quantum numbers to the eigenstates to use the spin−orbit coupled diabatic basis $|j_A\omega_A\rangle$ constructed in eq 4 of paper 1. The spin−orbit coupling term $A\hat{\boldsymbol{\lambda}} \hat{\mathbf{S}}$ in the Hamiltonian is diagonal in this basis, see paper 1. The total (electronic) atomic angular momentum of Br takes on the values $j_A = (^1/_2)$ with projections $\omega_A = \pm(^1/_2)$ on the dimer z axis and $j_A = (^3/_2)$ with projections $\omega_A = \pm(^1/_2), \pm(^3/_2)$.

The full three-dimensional BF basis is

$$|n_R, n_r, j_A, \omega_A, j_B, \omega_B, \Omega, J, M\rangle = \chi_{n_r}(R) \phi_{n_r}(r_{CH})$$

$$\left[\frac{2J+1}{4\pi}\right]^{1/2} |j_A, \omega_A\rangle Y_{j_B,\omega_B}(\theta,0) D_{M,\Omega}^{(J)}(\alpha,\beta,\phi)^* \quad (3)$$

where $Y_{j_B,\omega_B}(\theta,0)$ are spherical harmonics and $D_{M,\Omega}^{(J)}(\alpha,\beta,\phi)^*$ are symmetric rotor functions. The Euler angles (α,β,ϕ) determine the orientation of the BF frame with respect to a space-fixed laboratory frame. The kets $|j_A\omega_A\rangle$ denote the spin−orbit coupled diabatic electronic states. The quantum numbers j_B,ω_B refer to the rotation of the HCN monomer in the complex, with ω_B being the projection of j_B on the BF z axis. The quantum number $\Omega = \omega_A + \omega_B$ is the total projection of the atomic $\hat{\mathbf{j}}_A$ and molecular $\hat{\mathbf{j}}_B$ angular momenta on the BF z axis. All of these are approximate quantum numbers. Exact quantum numbers are the total angular momentum of the complex, J, its projection, M, on the space-fixed z axis, and the parity, p, under inversion. In the actual calculations, we used a parity-adapted basis, cf. eq 6 of ref 13. The spectroscopic parity is defined by $\epsilon = p(-1)^{J-S}$. States with $\epsilon = 1$ and $\epsilon = -1$ are labeled e and f, respectively.

In addition to the three-dimensional (3D) calculations, we made one-dimensional (1D) and two-dimensional (2D and 2+1D) calculations. The 1D calculations were made for fixed R values ranging from 6 to $16a_0$ and r_{CH} frozen at the experimental CH equilibrium distance 2.0135 a_0. The functions $|n_R\rangle$ and $|n_r\rangle$ were left out of the basis, and the radial kinetic energy terms were omitted. The HCN rotational constant in these
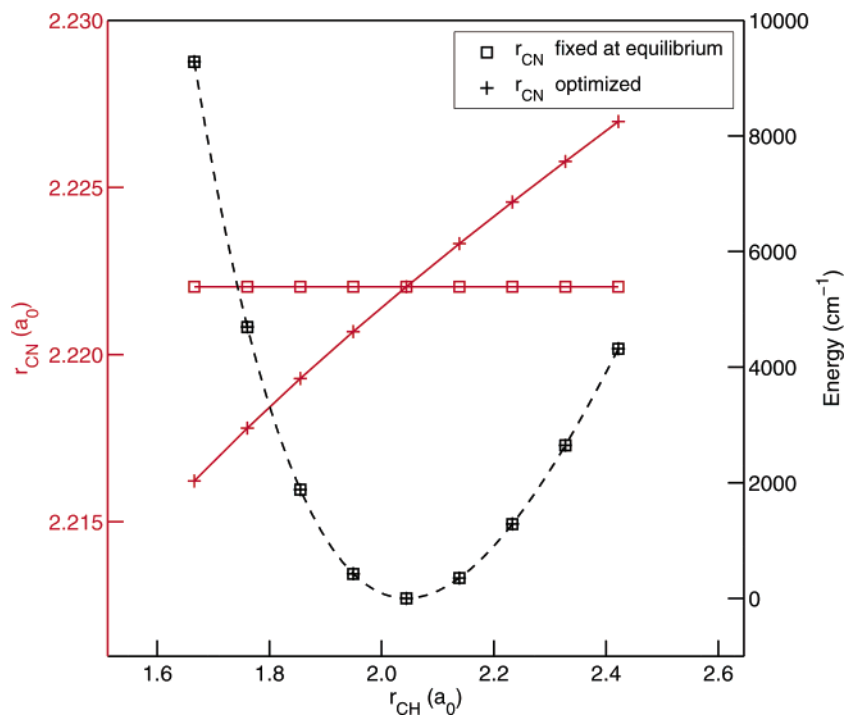
Figure 1. Energy of HCN as function of the CH bond length with the CN bond length frozen or optimized. Notice that the two energy curves coincide. The scale on the left-hand side is the CN bond length.

calculations was $B_0 = 1.47822$ cm^{-1}.[19] In the 2D calculations, we fixed r_{CH} at the equilibrium value of 2.0135 a_0 or at the vibrationally averaged values of $r_0 = 2.04099a_0$ for $v = 0$ and $r_1 = 2.09900a_0$ for $v = 1$, and omitted the basis $|n_r\rangle$ and the corresponding radial kinetic energy term. With $r_{CH} = 2.0135a_0$ and $2.04099a_0$, we used the HCN rotational constant $B_0 = 1.47822$ cm^{-1}; with $r_{CH} = 2.09900a_0$, we used $B_1 = 1.46774$ cm^{-1}. In the 2+1D calculations, we first averaged the full three-dimensional potentials over the CH stretch coordinate r_{CH} with the $v = 0$ or $v = 1$ CH stretch functions of HCN. Next, we performed two-dimensional calculations with the $v = 0$ or $v = 1$ averaged potentials and the correspondingly averaged rotational constants $B_0 = 1.478474$ cm^{-1} and $B_1 = 1.46535$ cm^{-1} of HCN. One may observe that the latter values of B_v differ slightly from the experimental values used in the 1D and 2D calculations. The reason is that our 2+1D values were computed with the CN bond length fixed at the equilibrium distance. The 2+1D model is equivalent to a full 3D calculation with the basis $|n_r\rangle$ restricted to a single function with either $n_r = 0$ or $n_r = 1$ because the basis $|n_r\rangle$ consists of eigenfunctions of the monomer Hamiltonian $\hat{H}_{HCN}$.

The 3D calculations were limited to $J = (^1/_2)$ and $(^3/_2)$, whereas in the 2+1D model we computed the rovibronic states for $J = (^1/_2)$, $(^3/_2)$, $(^5/_2)$, and $(^7/_2)$. In all calculations we performed a full diagonalization of the Hamiltonian matrix in the given parity-adapted basis. In 3D calculations, the lower levels of the complex correspond to $v = 0$ of the CH stretch mode; states that correspond to $v = 1$ of the CH stretch are much higher in energy and were identified among the highly excited intermolecular modes by a population analysis of the eigenstates. In the 2D calculations, we truncated the basis at $n_R^{max} = 17$ and $j_B^{max} = 17$. In the 2+1D model, we truncated at $n_R^{max} = 16$ and $j_B^{max} = 16$. In convergence studies, we found that an increase of each of these truncation parameters by 1, both in 2D and 2+1D, changed the ground state energy by less than 10^{-5} cm^{-1} and the somewhat higher levels by less than 10^{-4} cm^{-1}. In the full 3D model, we truncated at $n_R^{max} = 14$, $j_B^{max} =$

14 and $n_r^{max} = 4$. Here, the ground level changed by less than 10^{-3} cm^{-1} and the somewhat higher levels by less than 10^{-2} cm^{-1} if the truncation parameters are increased by 1. Energy differences, such as vibrational and rotational excitation energies, are converged significantly better, however.

3. Results and Discussion

3.1. Rovibronic Levels from 1D Calculations. The 1D calculations with fixed R and the CH distance frozen at the experimental equilibrium value of $2.0135a_0$ were made for parity e and total angular momentum $J = (^1/_2)$ and $J = (^3/_2)$. Figure 2 shows the calculated energy levels as functions of R in the range from $R = 6$ to $16a_0$. These curves correspond to the so-called adiabatic bender model of refs 24 and 25, which is extended here to include multiple coupled electronic states. To understand the behavior of these curves, it is useful to know that Ω, the projection of the total angular momentum J on the dimer z axis, is a nearly good quantum number. When the curves with $J = (^1/_2)$ and $J = (^3/_2)$ nearly coincide, this implies that the corresponding levels have $|\Omega| = (^1/_2)$. The energy difference between the curves with $J = (^3/_2)$ and $J = (^1/_2)$ involves only the overall rotation of the complex in that case. When a $J = (^3/_2)$ curve is well-separated from the $J = (^1/_2)$ curves, this implies that $|\Omega| = (^3/_2)$. Using this rule, we see that the deepest minimum at $R = 7.3a_0$ corresponds to a level with $|\Omega| = (^1/_2)$, whereas the second minimum at $R = 8.7a_0$ corresponds to a level with $|\Omega| = (^3/_2)$. Looking at the potential surfaces in Figures 4 and 5 of paper 1, one may guess that these two minima correspond to linear Br−NCH and linear Br−HCN, respectively. The latter has a much larger equilibrium distance, R_e, than the first one, but it seems to be about equally stable. One also observes a series of higher curves with minima at more or less the same distances, R. These correspond to a series of excited vibronic levels of either Br−NCH or or Br−HCN with $|\Omega|$ values that are sometimes different from their ground-state levels. These excited levels are combinations of bend excited states with $\omega_B \neq 0$ and the electronic states with $\omega_A = \pm(^1/_2)$
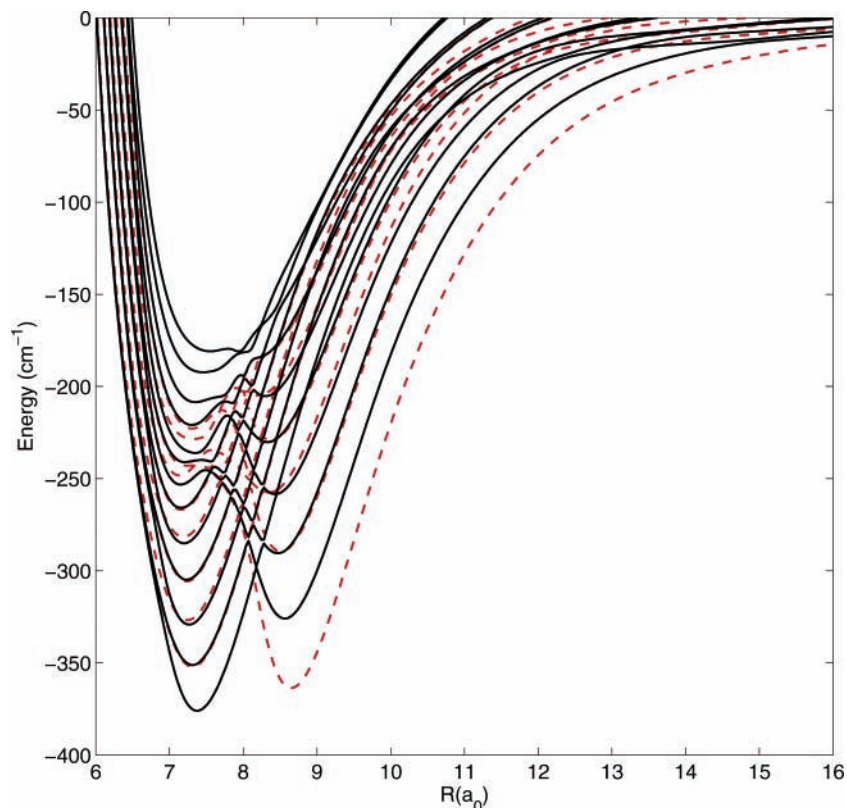
2. Bound-State Calculations and Infrared Spectra

J. Phys. Chem. A, Vol. 111, No. 31, 2007 **7273**

Figure 2. Rovibronic levels from 1D calculations with R and $r_{CH} = r_e$ fixed, as functions of R. Closed lines correspond to $J = (^1/_2)$, and dashed lines correspond to $J = (^3/_2)$.

and $\pm(^3/_2)$. Their $|\Omega|$ values follow directly from these quantum numbers because $\Omega = \omega_A + \omega_B$. The ground state has $\omega_B = 0$ and, hence, $\Omega = \omega_A$. Asymptotically, these levels correlate with the fourfold degenerate $^2P_{3/2}$ ground state of the Br atom and the ground and excited rotational levels of HCN. The results from the 2D and 3D calculations discussed below provide more details.

3.2. Rovibronic Levels from 2D and 3D Calculations. Before we discuss the results of the 2D, 2+1D, and 3D calculations, let us mention that the rovibronic wave functions (discussed below) clearly show that all states up to an energy of about 106 cm^{-1} above the ground level are localized either near the linear Br−NCH geometry ($\theta = 0°$) or near the linear Br−HCN geometry ($\theta = 180°$). Some of the higher excited levels below this limit show large-amplitude bend motions, but it is quite obvious that they belong to either Br−NCH or Br−HCN. Hence, we will discuss the properties of each of these isomers.

The binding energies D_0 of Br−NCH and Br−HCN computed with the different models are listed in Table 1. Clearly, the binding energy of Br−NCH depends only slightly on the model and on the CH stretch mode being excited or not, whereas D_0 of Br−HCN is much more sensitive. This can be understood from the result in paper 1 that the D_e and R_e values of Br−HCN depend more strongly on the length of the CH bond than the D_e and R_e values of Br−NCH. This, again, is reasonable because the CH bond is in direct contact with the Br atom in linear Br−HCN, whereas it is on the other side in linear Br−NCH. The 2+1D model with the 3D potentials averaged over the $v = 0$ or $v = 1$ wave functions of the CH stretch mode is much closer to the full 3D results than the 2D model with r_{CH} fixed at r_0 or r_1. A similar conclusion was drawn for Cl−HF.[13] Another conclusion, which is quite striking, is that the binding

energies of Br−NCH and Br−HCN differ by as little as 3.3 cm^{-1} (in the 3D model).

Tables 2 and 3 show the rovibronic levels of Br−NCH and Br−HCN, respectively, for the $v = 0$ ground state of the CH stretch mode, total angular momentum $J = (^1/_2)$ to $(^7/_2)$, and spectroscopic parity e. For $J = (^1/_2)$ and $(^3/_2)$, we also included the full 3D results in these tables. In accordance with the spectroscopic convention[26] for linear open-shell molecules, we labeled the levels with the term symbols $^{2S+1}K_P$. The vibronic quantum number K corresponds to the sum of the electronic orbital angular momentum usually denoted by Λ and the vibrational angular momentum of the bend mode commonly labeled by l. In our treatment, which includes the full range of angles θ, the relevant electronic angular momentum quantum number is μ, with the value $\mu = 0$ for the Σ ground state of linear Br−NCH and the values $\mu = \pm 1$ for the Π ground state of linear Br−HCN. The vibrational angular momentum, l, is given by ω_B. Hence, the quantum number, K, is given by $K = \mu + \omega_B$, which can also be written as $K = \Omega - \Sigma = \omega_A + \omega_B - \Sigma$, where $\Sigma = \pm(^1/_2)$ is the component of the spin S on the intermolecular z axis, R. The quantum number that is commonly denoted by P corresponds to $|\Omega|$ in our case. The ground state of Br−NCH with $|\Omega| = (^1/_2)$ corresponds to $K = 0$ and can be written in the spectroscopic notation[26] as $^2\Sigma_{(1/2)}$. The ground state of Br−HCN with $|\Omega| = (^3/_2)$ has $|K| = 1$ and can be written as $^2\Pi_{(3/2)}$. Because $|\Omega|$ is a nearly good quantum number, the energy levels in these tables are sorted according to their $|\Omega|$ values. The rows of levels with the same $|\Omega|$ and increasing values of $J \geq |\Omega|$ are end-over-end rotational progressions of the same internal state of the complex. Actually, the levels of Br−NCH and Br−HCN originate from a single calculation for each value of J. We could clearly assign the levels to either Br−NCH or Br−HCN on the basis of the electronic angular
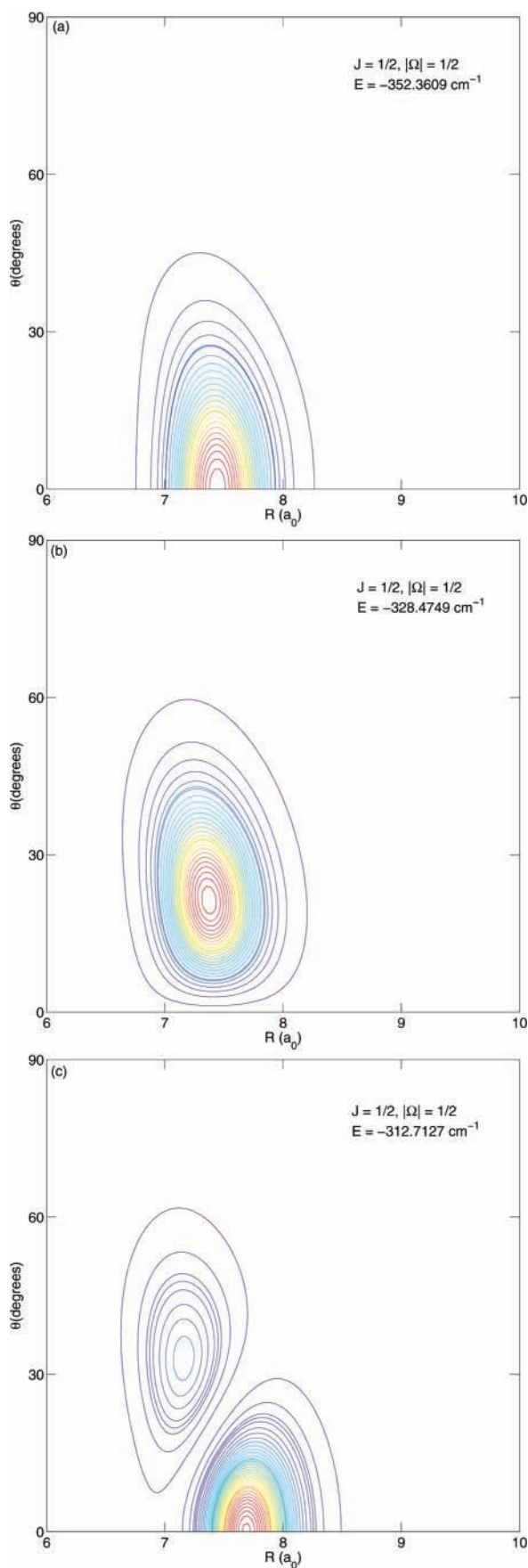
Figure 3. Density distributions corresponding to the Br–NCH conformation from the 2+1D model for $v_{CH} = 0$. They are obtained by integration of the squared absolute wave functions over the electronic coordinates and over all rotation angles (α, β, ϕ) of the complex. The energies and quantum numbers correspond to those in Table 2.

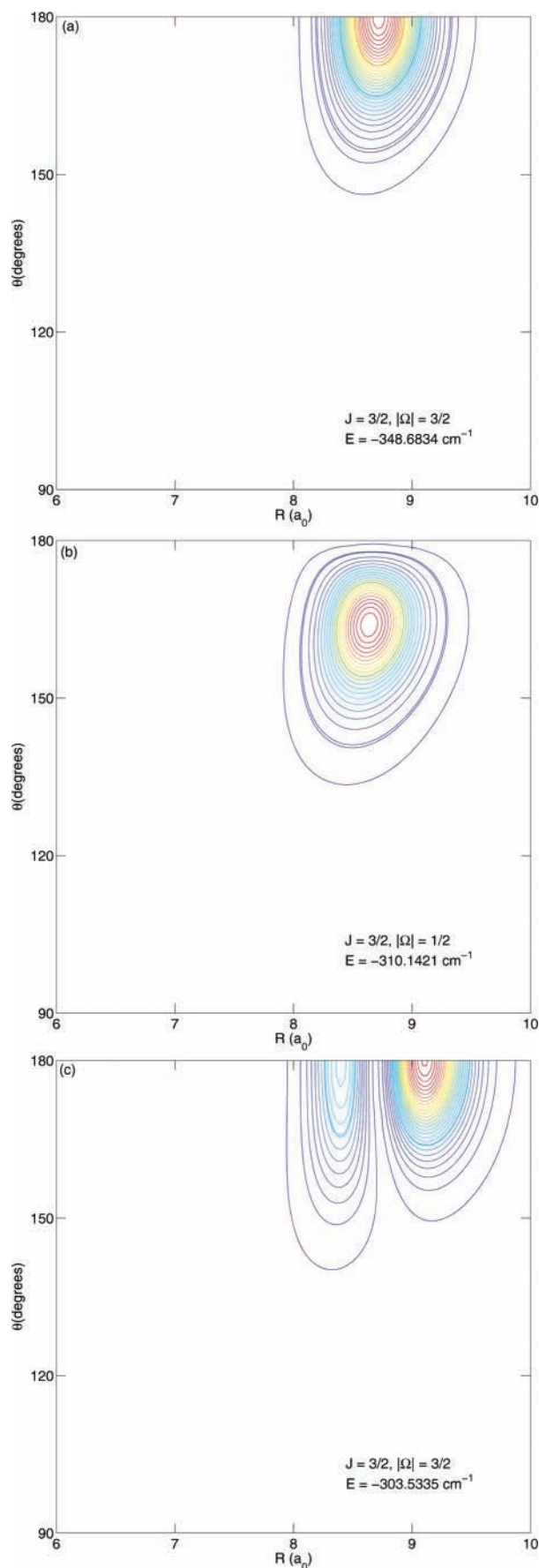**Figure 4.** Density distributions corresponding to the Br–HCN conformation from the 2+1D model for $v_{CH} = 0$. For details, see the caption of Figure 3. The energies and quantum numbers correspond to those in Table 3.

2. Bound-State Calculations and Infrared Spectra

J. Phys. Chem. A, Vol. 111, No. 31, 2007 **7275**

TABLE 1: Binding Energies D_0 (parity e) and Red Shifts of the CH Stretch Frequency Relative to Free HCN (in cm^{-1})

	Br–NCH ($J = (^1/_2)$)			Br–HCN ($J = (^3/_2)$)		
model	$v_{CH} = 0$	$v_{CH} = 1$	red shift	$v_{CH} = 0$	$v_{CH} = 1$	red shift
2D (r_e)	351.78			339.52		
2D	352.54	354.16	1.62	345.66	359.29	13.63
2+1D	352.36	354.33	1.97	348.68	371.52	22.84
3D	352.37	354.35	1.98	349.11	372.22	23.11
experiment[5]			1.65			26.59/23.80[a]

^{a} The latter value is corrected for the He matrix shift, see the text.

momentum projection $|\omega_A|$, which turns out to be $(^1/_2)$ for the ground state of Br–NCH and $(^3/_2)$ for the ground state of Br–HCN. Also, on the basis of the rovibronic wave functions being localized near either one the linear equilibrium geometries we could make such a distinction. Examples are shown in Figure 3 for Br–NCH and Figure 4 for Br–HCN. Actually, we did not plot the wave functions in these figures but rather the density distributions obtained by taking the absolute square of the wave function and integrating over the electronic coordinates and the overall rotation angles.

The density distributions as shown in Figures 3 and 4 can also be used to assign the vibrational quantum numbers v_s and v_b of the complex. The quantum number v_s refers to the Br–HCN or Br–NCH stretch mode in the coordinate R; the quantum number v_b refers to the bend mode of the linear complexes. The quantum number ω_B is the vibrational angular momentum of the bend mode. This quantum number and the electronic angular momentum projection, ω_A, occur in the diabatic basis used. In the complex, they are approximate quantum numbers and were obtained by a population analysis of the eigenstates. When the values of ω_A and ω_B are given in the tables, this implies that the eigenstates have more than 50% (in most cases much more) of this character. In the assignment of the bend quantum number v_b, the rule that ω_B runs from $-v_b$ to v_b by

steps of 2 was very helpful. The upper panel in Figure 3 is clearly the ground rovibronic state of Br–NCH, the middle panel is the bend fundamental, and the lower panel is the bend overtone mixed with the stretch fundamental in a Fermi resonance. In Figure 4, the upper panel is the ground rovibronic state of Br–HCN, the middle panel is the bend fundamental of that complex, and the lower panel is the pure stretch fundamental in this case.

In Table 2, one reads that the ground state of Br–NCH with approximate quantum numbers $\omega_B = v_b = v_s = 0$ and energy $E = -352.37$ cm^{-1} occurs for $J = |\Omega| = (^1/_2)$ and is dominated by the diabatic state with $j_A = (^3/_2)$ and $|\omega_A| = (^1/_2)$. The fundamental bend frequency of Br–NCH is 23.0 or 23.9 cm^{-1}, depending on whether one considers the $|\Omega| = (^3/_2)$ or the $|\Omega| = (^1/_2)$ bend excited level. The density distribution in the middle panel of Figure 3 corresponds to the latter level, but the distribution of the former state (not shown) is almost indistinguishable. The only difference between these states is that the electronic angular momentum $\omega_A = \pm(^1/_2)$ is coupled parallel or antiparallel to the bend angular momentum $\omega_B = \pm 1$. Because the spin-free ground state of Br–NCH is a Σ state, see paper 1, the value of $\omega_A = \pm(^1/_2)$ is purely determined by the projection of the spin $S = (^1/_2)$ on the dimer axis. The orbital angular momentum vanishes for a Σ state, there is only a small indirect Renner–Teller coupling, and the two bend frequencies are very nearly the same. In Section 3.4, we will discuss this in more detail. The modes at 39.7 and 51.5 cm^{-1} are the bend overtone and the stretch fundamental, but according to the density distributions these are mixed into a Fermi resonance. In Table 3, one can see that the ground state of Br–HCN has $J = |\Omega| = (^3/_2)$ and energy $E = -349.11$ cm^{-1}. It is dominated by the diabatic state with $j_A = |\omega_A| = (^3/_2)$. The bend fundamental frequency, 38.7 cm^{-1}, of Br–HCN is considerably higher than that for Br–NCH. This value is derived from the bend excited level with $|\Omega| = (^1/_2)$; the bend excited level with

TABLE 2: Lowest Bound States of e Parity of Br–NCH ($\theta = 0°$) from the 2+1D Model with $v_{CH} = 0^a$

term	$|\omega_A|$	$|\omega_B|$	v_b	v_s	$J = (^1/_2)$		$J = (^3/_2)$		$J = (^5/_2)$	$J = (^7/_2)$
						$\|\Omega\| = (^1/_2)$				
$^2\Sigma_{(1/2)}$	0.5	0	0	0	−352.3609	(−352.3701)	−352.3044	(−352.3136)	−352.1428	−351.8762
$^2\Pi_{(1/2)}$	0.5	1	1	0	−328.4749	(−328.4850)	−328.2843	(−328.2945)	−327.9690	−327.5328
$^2\Sigma_{(1/2)}$	0.5	0	2	0	−312.7127	(−312.7229)	−312.6530	(−312.6632)	−312.4857	−312.2108
$^2\Sigma_{(1/2)}$	0.5	0	0	1	−300.9041	(−300.9133)	−300.8471	(−300.8564)	−300.6863	−300.4217
$^2\Pi_{(1/2)}$	0.5	1	3	0	−291.3396	(−291.3506)	−291.1451	(−291.1562)	−290.8230	−290.3774
$^2\Pi_{(1/2)}$	0.5	1	1	1	−276.3575	(−276.3672)	−276.1714	(−276.1812)	−275.8630	−275.4356
$^2\Sigma_{(1/2)}$	0.5	0	4	0	−274.7948	(−274.8064)	−274.7317	(−274.7433)	−274.5584	−274.2751
$^2\Sigma_{(1/2)}$	0.5	0	0	2	−264.3586	(−264.3680)	−264.2987	(−264.3081)	−264.1335	−263.8630
$^2\Pi_{(1/2)}$	0.5	1	5	0	−254.8922	(−254.9048)	−254.6932	(−254.7058)	−254.3637	−253.9075
$^2\Sigma_{(1/2)}$	0.5	0	2	1	−253.0965	(−253.1052)	−253.0373	(−253.0461)	−252.8747	−252.6084
						$\|\Omega\| = (^3/_2)$				
$^2\Pi_{(3/2)}$	0.5	1	1	0			−329.2981	(−329.3082)	−329.0794	−328.7670
$^2\Delta_{(3/2)}$	0.5	2	2	0			−304.6535	(−304.6649)	−304.3525	−303.9325
$^2\Pi_{(3/2)}$	0.5	1	3	0			−292.1430	(−292.1540)	−291.9203	−291.6022
$^2\Pi_{(3/2)}$	0.5	1	1	1			−277.2085	(−277.2182)	−276.9904	−276.6798
$^2\Delta_{(3/2)}$	0.5	2	4	0			−268.6951	(−268.7074)	−268.3888	−267.9614
$^2\Pi_{(3/2)}$	0.5	1	5	0			−255.7079	(−255.7169)	−255.4971	−255.1776
$^2\Delta_{(3/2)}$	0.5	2	2	1			−253.7150	(−253.7256)	−253.4211	−253.0107
						$\|\Omega\| = (^5/_2)$				
$^2\Delta_{(5/2)}$	0.5	2	2	0					−306.2819	−305.9371
$^2\Phi_{(5/2)}$	0.5	3	3	0					−280.1198	−279.7050
$^2\Delta_{(5/2)}$	0.5	2	4	0					−270.3068	−269.9553
$^2\Delta_{(5/2)}$	0.5	2							−255.4390	−255.0877
						$\|\Omega\| = (^7/_2)$				
$^2\Phi_{(7/2)}$	0.5	3	3	0						−282.5384

^{a} Energies in cm^{-1} relative to the energy of Br (^{2}P$_{3/2}$) and HCN($v_{CH} = 0$). The numbers in parentheses are from 3D calculations. Quantum numbers v_s and v_b refer to the intermolecular stretch and bend. The approximate quantum numbers ω_A and ω_B and the term symbol $^{2S+1}K_{|\Omega|}$ are explained in the text.

TABLE 3: Lowest Bound States of e Parity of Br−HCN ($\theta = 180°$) from the 2+1D Model with $v_{CH} = 0^a$

term	$|\omega_A|$	$|\omega_B|$	v_b	v_s	$J = (^1/_2)$		$J = (^3/_2)$		$J = (^5/_2)$	$J = (^7/_2)$
					$|\Omega| = (^1/_2)$					
$^2\Sigma_{(1/2)}$	1.5	1	1	0	−310.2585	(−310.5624)	−310.1421	(−310.4459)	−309.9472	−309.6737
$^2\Pi_{(1/2)}$	1.5	2	2	0	−274.4774	(−274.6776)	−274.3567	(−274.5568)	−274.1554	−273.8737
$^2\Sigma_{(1/2)}$	1.5	1	1	1	−269.7106	(−269.8983)	−269.5947	(−269.7823)	−269.4000	−269.1266
					$|\Omega| = (^3/_2)$					
$^2\Pi_{(3/2)}$	1.5	0	0	0			−348.6834	(−349.1115)	−348.4911	−348.2218
$^2\Pi_{(3/2)}$	1.5	0	0	1			−303.5335	(−303.7839)	−303.3443	−303.0795
$^2\Pi_{(3/2)}$	1.5	0	2	0			−276.2600	(−276.2378)	−276.0613	−275.7832
$^2\Pi_{(3/2)}$	1.5	0	0	2			−258.4154	(−255.9429)	−258.2300	−257.9705
					$|\Omega| = (^5/_2)$					
$^2\Delta_{(5/2)}$	1.5	1	1	0					−307.3673	−307.0928
$^2\Delta_{(5/2)}$	1.5	1	1	1					−266.9047	−266.6289
					$|\Omega| = (^7/_2)$					
$^2\Phi_{(7/2)}$	1.5	2	2	0						−268.8726

^{a} Energies in cm^{-1} relative to the energy of Br ($^2P_{3/2}$) and HCN ($v_{CH} = 0$). The numbers in parentheses are from 3D calculations. For an explanation of the symbols, see Table 2.

TABLE 4: Bend and Stretch Frequencies (in cm^{-1}) of Br−NCH and Br−HCN for $v_{CH} = 0$ and 1

	Br−NCH			Br−HCN	
transition	$v_{CH} = 0$	$v_{CH} = 1$	transition	$v_{CH} = 0$	$v_{CH} = 1$
	fundamental bend frequency				
$^2\Sigma_{(1/2)} \rightarrow {}^2\Pi_{(1/2)}$	23.9	23.7	$^2\Pi_{(3/2)} \rightarrow {}^2\Sigma_{(1/2)}$	38.5	43.4
$^2\Sigma_{(1/2)} \rightarrow {}^2\Pi_{(3/2)}$	23.0	22.9	$^2\Pi_{(3/2)} \rightarrow {}^2\Delta_{(5/2)}$	41.1	46.2
	fundamental stretch frequency				
$^2\Sigma_{(1/2)} \rightarrow {}^2\Sigma_{(1/2)}$	51.5	51.4	$^2\Pi_{(3/2)} \rightarrow {}^2\Pi_{(3/2)}$	45.1	47.6

$|\Omega| = (^5/_2)$ gives a bend fundamental frequency of 41.1 cm^{-1}. As will be discussed in Section 3.4, this difference can be explained by the Renner−Teller nonadiabatic coupling of the bend mode to the electronic angular momentum, ω_A, of the Π ground state of Br−HCN. The stretch fundamental frequency of Br−HCN is 45.3 cm^{-1}, not much different from Br−NCH. From these tables, one can also read the frequencies of the bend overtone with $v_b = 2$, which has two components, one with $\omega_B = 0$ and one with $|\omega_B| = 2$. The differences between the frequencies of these components are about 2 cm^{-1}; they are caused by the anharmocity of the bending potentials. Also, bend−stretch combination levels and overtones can be observed. We already mentioned that in Br−NCH the bend overtone and stretch fundamental mix into a Fermi resonance. Similar resonances occur between the second and third bend overtone and the corresponding modes with two bend quanta replaced by one stretch quantum.

Looking back at the "adiabatic bender" curves from the 1D calculations in Figure 2, we may now conclude that the minimum at $R = 7.3a_0$ in the lowest two nearly coinciding curves with $|\Omega| = (^1/_2)$ indeed correspond to linear Br−NCH. The minimum at $R = 8.7a_0$ in the lowest curve with $J = |\Omega| = (^3/_2)$ represents linear Br−HCN.

The results calculated with the CH stretch mode excited to $v = 1$ are qualitatively similar to those obtained for $v = 0$. Therefore, we do not show all of the levels. In Table 1, one could see already that the complex becomes more strongly bound when the CH stretch mode is excited and that this effect is much more important for Br−HCN than for Br−NCH. The bend and stretch fundamental frequencies of both complexes are listed in Table 4. One notices there that in Br−HCN the bend and stretch frequencies are also higher for $v = 1$ than for $v = 0$. In Br−NCH, there are hardly any differences between $v = 0$ and $v = 1$.

Table 5 for Br−NCH and Table 6 for Br−HCN contain the parity splittings between the levels of e and f symmetry. The splittings $E_f - E_e$ are by far the largest for the $|\Omega| = (^1/_2)$ levels with $\omega_B = 0$ in Br−NCH and they increase linearly with $J + (^1/_2)$. This simple linear dependence on $J + (^1/_2)$ is well-known for λ doubling in linear molecules,[27] and it was also found in Cl(^2P)−HCl[10,11,17] and Cl(^2P)−HF.[13] The parity-splitting characteristics can be understood by considering the Hamiltonian in eq 1 and the basis in eq 3. The energy difference between functions with e and f parity is caused by a coupling between the basis components with (ω_A, ω_B, Ω) and ($-\omega_A$, $-\omega_B$, $-\Omega$). The term in the Hamiltonian that is responsible for this coupling is the Coriolis coupling operator $-2(\hat{\jmath}_A + \hat{\jmath}_B)\cdot\hat{J}/(2\mu_{AB}R^2)$ and, in particular, the step-up and step-down terms with $\hat{\jmath}_A^+\hat{J}^+$ and $\hat{\jmath}_A^-\hat{J}^-$ in this operator. The step-up and step-down operators $\hat{\jmath}_B^\pm\hat{J}^\pm$ cannot directly couple basis functions with ω_B and $-\omega_B$ because this quantum number has integer values and the step-up and step-down operators shift ω_B only by ± 1. The terms $\hat{\jmath}_A^\pm\hat{J}^\pm/(2\mu_{AB}R^2)$ couple basis functions with (ω_A,ω_B,Ω) = (($^1/_2$),0,($^1/_2$)), and ($-(^1/_2)$,0, $-(^1/_2)$). The coupling matrix elements are

$$[(j_A(j_A + 1) - \omega_A(\omega_A \pm 1))(J(J + 1) -$$
$$\Omega(\Omega \pm 1))]^{1/2}\langle[2\mu_{AB}R^2]^{-1}\rangle = \left(j_A + \frac{1}{2}\right)\left(J + \frac{1}{2}\right)\langle[2\mu_{AB}R^2]^{-1}\rangle$$

(4)

and they cause a first-order splitting between the levels of e and f parity, which would otherwise be degenerate. Equation 4 shows that this splitting should indeed be proportional to $J + (^1/_2)$ with a proportionality constant that is $2(j_A + (^1/_2))$ times the expectation value of $[2\mu_{AB}R^2]^{-1}$ over the radial part of the wavefunction. Because of the very large spin−orbit splitting between the $^2P_{1/2}$ and $^2P_{3/2}$ states of the Br atom, the quantum number j_A is nearly ($^3/_2$) in the lower levels of the complex. The expectation value $\langle[2\mu_{AB}R^2]^{-1}\rangle$ is the end-over-end rotational constant B. Hence, the splitting should be about $4B(J + (^1/_2))$, with $B = 0.0525$ cm^{-1} for Br−NCH (see below). This is indeed what we see in Table 5 for the levels with $\omega_B = 0$ and $|\Omega| = (^1/_2)$ of Br−NCH because $|\omega_A| = (^1/_2)$ in this isomer. Functions with $\omega_B = \pm 1$ are only coupled indirectly through functions with $\omega_B = 0$ and show a small parity splitting. For $|\Omega| = (^3/_2)$, the splittings are even smaller and they are proportional to $(J - (^1/_2))(J + (^1/_2))(J + (^3/_2))$ as pointed out by Dubernet and Hutson.[17] They are due to a higher-order effect of the Coriolis coupling operator $\hat{\jmath}_A^\pm\hat{J}^\pm/(2\mu_{AB}R^2)$. In Br−HCN, which has $|\omega_A| = (^3/_2)$, the splitting is smaller by several orders of magnitude than in Br−NCH and is proportional to $J + (^1/_2)$,

2. Bound-State Calculations and Infrared Spectra

J. Phys. Chem. A, Vol. 111, No. 31, 2007 **7277**

TABLE 5: Parity Splittings $\Delta E = E_f - E_e$ in cm^{-1} of Br$-$NCH ($\theta = 0°$) for $v_{CH} = 0$

$|\omega_A|$	$|\omega_B|$	v_b	v_s	$J = (^1/_2)$		$J = (^3/_2)$		$J = (^5/_2)$	$J = (^7/_2)$
				$|\Omega| = (^1/_2)$					
0.5	0	0	0	0.2022	(0.2022)	0.4043	(0.4043)	0.6064	0.8085
0.5	1	1	0	0.0045	(0.0045)	0.0084	(0.0084)	0.0113	0.0132
0.5	0	2	0	0.2032	(0.2033)	0.4065	(0.4065)	0.6097	0.8128
0.5	0	0	1	0.1977	(0.1977)	0.3954	(0.3954)	0.5931	0.7908
0.5	1	3	0	0.0055	(0.0055)	0.0100	(0.0101)	0.0130	0.0143
0.5	1	1	1	0.0042	(0.0042)	0.0076	(0.0076)	0.0099	0.0109
0.5	0	4	0	0.2043	(0.2043)	0.4085	(0.4085)	0.6127	0.8168
0.5	0	0	2	0.1961	(0.1961)	0.3921	(0.3921)	0.5881	0.7841
0.5	1	5	0	0.0040	(0.0040)	0.0065	(0.0066)	0.0068	0.0046
0.5	0	2	1	0.1921	(0.1921)	0.3842	(0.3842)	0.5762	0.7681
				$|\Omega| = (^3/_2)$					
0.5	1	1	0			0.0006	(0.0006)	0.0022	0.0048
0.5	2	2	0			0.0000	(0.0000)	0.0000	0.0000
0.5	1	3	0			0.0010	(0.0010)	0.0035	0.0078
0.5	1	1	1			0.0007	(0.0007)	0.0027	0.0059
0.5	2	4	0			0.0000	(0.0000)	0.0000	0.0000
0.5	1	5	0			0.0014	(0.0014)	0.0033	0.0075
0.5	2	2	1			0.0000	(0.0000)	0.0001	0.0002

TABLE 6: Parity Splittings $\Delta E = E_f - E_e$ in cm^{-1} of Br$-$HCN ($\theta = 180°$) for $v_{CH} = 0$[a]

$|\omega_A|$	$|\omega_B|$	v_b	v_s	$J = (^1/_2)$		$J = (^3/_2)$		$J = (^5/_2)$	$J = (^7/_2)$
				$|\Omega| = (^1/_2)$					
1.5	1	1	0	0.0027	(0.0027)	0.0054	(0.0054)	0.0082	0.0109
1.5	2	2	0	0.0000	(−0.0001)	0.0000	(−0.0001)	−0.0001	−0.0001
1.5	1	1	1	0.0047	(0.0046)	0.0093	(0.0093)	0.0140	0.0186

[a] For $|\Omega| \geq (^3/_2)$, all splittings are less than 10^{-4} cm^{-1}.

TABLE 7: Spectroscopic Parameters (in cm^{-1}) from the 2+1D Model

	Br$-$NCH ($\theta = 0°$)		Br$-$HCN ($\theta = 180°$)	
	$v_{CH} = 0$	$v_{CH} = 1$	$v_{CH} = 0$	$v_{CH} = 1$
	intermolecular stretch			
E_e	−383.58	−385.53	−371.27	−395.51
ω_e	66.36	66.33	45.18	48.11
$\omega_e x_e$	7.46	7.45	0.016	0.26
	rotational constants			
E_0	−352.29	−354.25	−348.74	−371.58
B	0.05253	0.05254	0.03847	0.03846
D	$3.8 \ 10^{-7}$	$2.5 \ 10^{-7}$	$2.4 \ 10^{-7}$	$2.4 \ 10^{-7}$

see Table 6. The splittings are only shown for $v = 0$ of the CH stretch mode; the results for $v = 1$ are very similar.

3.3. Spectroscopic Parameters. Only short stretch progressions with $v_s \leq 2$ can be seen in Table 2 for Br$-$NCH and Table 3 for Br$-$HCN. When we fitted these to the usual anharmonic oscillator formula, as we did for Cl$-$HF,[13] we found the harmonic stretch frequencies ω_e and anharmonicity constants $\omega_e x_e$ given in Table 7. For Br$-$NCH, the stretch mode shows a large anharmonicity. This is an effect of the Fermi resonance with the bend overtone that we already observed. In Br$-$HCN, the anharmonicity is very small.

From the series of levels calculated for $J = (^1/_2)$ to $(^7/_2)$ with the 2+1D model, we computed rotational constants, B, and distortion constants, D, by a fit to the linear molecule expression

$$E(J) = E_0 + B[J(J+1) - \Omega^2] - D[J(J+1) - \Omega^2]^2 \quad (5)$$

This formula was applied after averaging the energies over the levels of parities e and f. The results for the ground state of each isomer are given in Table 7. One observes in this table that the rotational constants of Br$-$NCH and Br$-$HCN are quite different. One also observes that excitation of the CH stretch mode has only a small effect on the rotational constant of the complex. This effect is probably reduced because of two opposing phenomena. When the CH stretch is excited the complex becomes more strongly bound, which tends to decrease the value of the equilibrium distance, R_e. Alternatively, the CH group becomes longer when it is excited, which will increase R_e through the repulsive interaction. This argument holds in particular for Br$-$HCN, but for Br$-$NCH the effect of the CH stretch is very small anyway.

From the energy difference between the lowest levels corresponding to $v = 0$ and $v = 1$ for the CH stretch mode, we extracted the red shift of the CH stretch frequency in the complex, relative to free HCN. The results of different models are included in Table 1. It is quite natural that the shift is much larger (23.11 cm^{-1}) for Br$-$HCN than for Br$-$NCH (1.98 cm^{-1}) because of the direct neighborhood of the Br atom to the CH group.

3.4. Renner$-$Teller Coupling. Linear Br$-$HCN is a typical Renner$-$Teller system[28] of case 1(a),[29] because (in the absence of spin$-$orbit coupling) it has a twofold degenerate electronic ground state of Π symmetry. When the complex bends the Π state splits into one A' and one A'' state with an energy difference that is nearly quadratic in the bend angle, see paper 1. The ground state of Br$-$HCN with $|\Omega| = (^3/_2)$ is written in Renner$-$Teller notation[26] as $^{2S+1}K_P = {}^2\Pi_{(3/2)}$. The same term symbol holds for the accompanying intermolecular stretch progression with v_s ranging from 0 to 2. Most interesting are the bend excited states with $v_b = 1$ and vibrational angular momentum $\omega_B = \pm 1$. They give rise to a bend fundamental with $|\Omega| = (^1/_2)$ denoted by $^2\Sigma_{(1/2)}$ and a bend fundamental with $|\Omega| = (^5/_2)$ denoted by $^2\Delta_{(5/2)}$. Both of these bend modes are indeed found, see Tables 3 and 4, as well as the accompanying bend$-$stretch combination levels. The fundamental bend frequency for the $^2\Sigma_{(1/2)}$ levels is 38.7 cm^{-1}, and for the $^2\Delta_{(5/2)}$ levels it is 41.1 cm^{-1}. For the levels that correspond to $v_{CH} = 1$, the $^2\Sigma_{(1/2)}$ bend frequency is 43.4 cm^{-1} and the $^2\Delta_{(5/2)}$ bend frequency is 46.2 cm^{-1}. These numbers are from the 2+1D calculations because

the 3D results are not available for $|\Omega| = (5/2)$. The value for the $^2\Sigma_{(1/2)}$ levels from 3D calculations is not very different, however.

We may compare our set of levels to the energy-level diagram of a $^2\Pi$ triatomic linear molecule shown in Herzberg's book,[26] Figure 8 of Section I.2. This diagram correlates the energy levels obtained from a full calculation with the levels obtained when either the Renner−Teller interaction or the spin−orbit coupling are set to zero. Herzberg's "full" treatment includes the bending mode only, and it defines the Renner−Teller interaction parameter, ϵ, as the ratio of the harmonic force constants of the coupling or difference potential $V_{1,-1} = [V(A'') - V_1(A')]/2$ at the linear geometry and the diagonal or sum potential $2V_{1,1} = V_1(A') + V(A'')$. Note that the bend quantum number, v_b, in our notation is denoted as v_2 in Herzberg's figure. In Herzberg's figure, the levels of the same $|K|$ with the larger P are higher than the levels with smaller P, whereas in our case the levels with the larger P are lower. The reason for this reversed order is that our spin−orbit constant, A, has a negative value, whereas Herzberg's is positive. In that sense, the Br−HCN results may be compared with the level patterns of some other Renner−Teller systems, Cl−HF[13] and He−HF+,[30] calculated in our group earlier. However, the absolute value of 2457 cm^{-1} of the spin−orbit parameter, A, in the Br atom is so large that the upper levels of the spin−orbit doublets in Br−HCN (such as the $^2\Pi_{(1/2)}$ level that is spin−orbit excited from the ground $^2\Pi_{(3/2)}$ level) are not bound anymore. Otherwise, the levels from our calculations follow the pattern of the levels in Herzberg's picture of a typical Renner−Teller system.

The splitting of 2.6 cm^{-1} between the $^2\Sigma_{(1/2)}$ and $^2\Delta_{(5/2)}$ levels that correspond to the same $v_b = 1$ bend fundamental is caused by the Renner−Teller interaction (parametrized in Herzberg's treatment by ϵ), which in our case is represented by the off-diagonal diabatic potential $V_{1,-1}$. This splitting is considerably smaller than the splitting of 38.6 cm^{-1} found for Cl−HF.[13] But the bend frequency of Br−HCN is also much lower than that for Cl−HF, and the spin−orbit coupling is much stronger. In the work on He−HF+,[30] it was shown that this splitting does not disappear even when the coupling potential $V_{1,-1}$ is switched off. This is a fundamental deviation from Herzberg's model, which was shown in ref 30 to be due to the fact that the bending motion is treated in our work as a hindered rotation rather than a harmonic vibration as in Renner's work.

Linear Br−NCH is not a Renner−Teller system because (in the absence of spin−orbit coupling) it has a nondegenerate electronic ground state of Σ symmetry. The spin−orbit coupling in the Br atom is very strong, however, and we discussed already in Section 4 of paper 1 that in the ground state of linear Br−NCH with approximate quantum numbers $j_A = (3/2)$ and $|\omega_A| = (1/2)$ the wave function has $1/3$ of Π character. Hence, it is interesting to look for effects similar to those of Renner−Teller coupling. We saw already in Section 3.2 that the fundamental bend frequency of Br−NCH is 23.0 or 23.9 cm^{-1}, depending on whether one considers the $|\Omega| = (3/2)$ or $|\Omega| = (1/2)$ bend excited state. The density distributions of these states are very similar. The only difference between them is that the electronic angular momentum $\omega_A = \pm(1/2)$ is coupled parallel or antiparallel to the bend angular momentum $\omega_B = \pm1$. So, there is a small indirect Renner−Teller splitting of 0.9 cm^{-1} in this case.

4. Comparison with Experiment

Experimentally,[5] both linear isomers, Br−NCH and Br−HCN, have been observed spectroscopically in a molecular beam

of He nanodroplets. It was found, in agreement with our results, that the ground state of Br−NCH has $|\Omega| = (1/2)$ and the ground state of Br−HCN has $|\Omega| = (3/2)$. For Br−NCH, a red shift of 1.65 cm^{-1} of the CH stretch frequency was observed, whereas for Br−HCN the red shift is 25.59 cm^{-1}. Before we compare with the shifts calculated for the complex in the gas phase, we should correct the experimental values for a possible matrix shift induced by the He clusters. A comparison of the shifts observed for several hydrogen-bonded complexes in the gas phase and in helium has shown[31] that there is indeed such a matrix effect and an empirical correction formula was proposed: $\Delta = 1.822 + 0.03655X$ cm^{-1},[5] where Δ is the correction that should be subtracted to obtain the gas-phase value of the red shift and X is the measured red shift in helium. We used this correction for Br−HCN, where the red shift is quite large. The shift after correction is 23.80 cm^{-1}, close to our computed value of 23.11 cm^{-1} (see Table 1). The correction formula was only derived for HX stretch frequencies in hydrogen-bonded complexes where HX is the donor, so the H atom is bound directly to the acceptor, and it cannot be applied to Br−NCH. Moreover, the shift found for Br−NCH is so small that the correction would give a negative shift and we omitted it in this case. The value of 1.98 cm^{-1} obtained from ab initio calculations with the full 3D model is in good agreement with the uncorrected experimental value of 1.65 cm^{-1}.

The ab initio-computed rotational constants of Br−NCH and Br−HCN are $B = 0.0525$ cm^{-1} and $B = 0.0385$ cm^{-1}, respectively. The experimental values are $B = 0.019$ cm^{-1} and $B = 0.0151$ cm^{-1}.[5] The measured values are smaller than the computed ones by factors of 2.8 and 2.5, respectively. These factors are in good agreement with literature values for various molecules in superfluid helium droplets.[31] They are caused by some of the surrounding helium atoms following the rotation of the molecule and, thus, increasing its effective moments of inertia.

In our calculations on Br−NCH, we predicted large parity splittings of the levels with $\omega_B = 0$, see Table 5. For the ground state of Br−NCH with $|\Omega| = (1/2)$, we predicted a splitting of 0.2022 cm^{-1} for $J = (1/2)$, which is about $4B = 0.210$ cm^{-1}. Such a splitting of about $4B$ that increases linearly with $J + (1/2)$ could be very-well rationalized by the theory in Section 3.2, see eq 4. The simulation of the measured spectrum in ref 5 gave a much smaller parity splitting. Taking into consideration the reduction of B by a factor of nearly 3 by the surrounding helium atoms, the experimental splitting is about $2B$. This would imply, according to our theory for this splitting in Section 3.2, that the quantum number $j_A = (3/2)$ in eq 4 must be replaced by $S = (1/2)$. In other words, only the spin is involved in the off-diagonal Coriolis coupling with the overall rotation of the complex, not the electronic orbital angular momentum. If this holds, and we fail to see any other explanation for the discrepancy between theory and experiment, then this must be an effect of the liquid-helium matrix.

The (side-)bands associated with the bend and stretch modes of the complex have not been observed yet. Therefore, we cannot compare our calculated results with experiment for these modes. It will be interesting to try and measure such modes.

5. Model Study of Cl−HCN, Role of Spin−Orbit Coupling

Also, the linear Cl−NCH complex was observed in a helium-droplet experiment by Merritt et al.,[5] but not the hydrogen-bonded Cl−HCN complex. To understand why both isomers
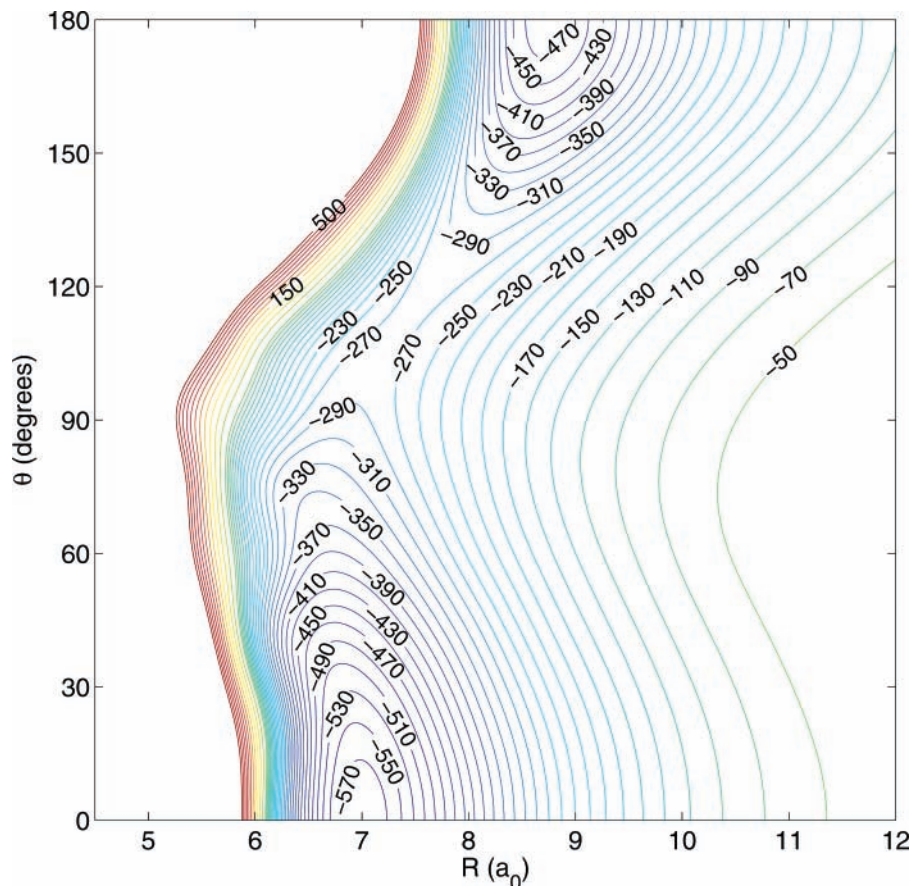
2. Bound-State Calculations and Infrared Spectra

J. Phys. Chem. A, Vol. 111, No. 31, 2007 **7279**

Figure 5. Lowest spin−orbit adiabatic potential energy surface for Cl(^{2}P)−HCN, obtained with the spin-free potentials of Br(^{2}P)−HCN and the spin−orbit coupling constant of Cl(^{2}P). Energy (in cm^{-1}) relative to the Cl(^{2}P$_{3/2}$) and HCN ground states.

were found for the complex of Br with HCN, and only a single one for the Cl complex, we made some exploratory calculations of the adiabatic potential surfaces for Cl−HCN. The potentials turned out to be qualitatively similar to those of Br−HCN. Even quantitatively, the differences are not very large. We found, for example, with the same RCCSD(T) method and the same basis as that used for Br−HCN that the value of D_e for the global X−NCH minimum in the lowest adiabatic potential is 726 cm^{-1} for X = Cl, whereas it was 800 cm^{-1} for X = Br. The local minimum for the linear X−HCN structure corresponds to D_e = 359 cm^{-1} for X = Cl and 415 cm^{-1} for X = Br. We realized, because the effect of spin−orbit coupling on the relative stability of the two isomers was so important for Br−HCN, see Section 4 of paper 1, that perhaps the differences between the Cl complex and the Br complex are caused mainly by the fact that the spin−orbit coupling is much smaller in Cl than in Br. To investigate this hypothesis, we made 2+1D bound state calculations for the Cl−HCN complex with the same potential surfaces as those used in our Br−HCN calculations. The only difference is that we introduced the spin−orbit splitting of 882.4 cm^{-1} between the ^{2}P$_{1/2}$ and ^{2}P$_{3/2}$ states of Cl instead of the corresponding splitting of 3685.5 cm^{-1} for Br. In addition, we used the reduced mass of Cl−HCN (with the Cl mass of 34.96885271 u) instead of that of Br−HCN, but this did not turn out to be important.

It is very interesting that we found, on the same potential surfaces, that the binding energy D_0 of linear Cl−NCH is 501.6 cm^{-1}, whereas it is only 344.9 cm^{-1} for linear Cl−HCN. The difference is 156.7 cm^{-1}, whereas the difference in D_0 between Br−NCH and Br−HCN is only 3.3 cm^{-1}. The Cl−NCH isomer that we find most stable is indeed the one observed.

We will now explain how spin−orbit coupling can cause such a largely different behavior. Let us look first at the plots of the potentials for the spin−orbit coupled diabatic states discussed in Section 4 of paper 1. One observes there that the minimum for linear Br−HCN in the spin−orbit coupled diabatic potential for the $j_A = (^3/_2)$ state with $|\omega_A| = (^3/_2)$ is the same as the minimum in the diabatic potential $V_{1,1}$ of the spin-free Π state. Alternatively, the minimum for Br−NCH in the potential for $|\omega_A| = (^1/_2)$ is much shallower than the corresponding minimum in the spin-free Σ state potential $V_{0,0}$. So, although Br−NCH has a much deeper minimum than Br−HCN in the spin-free case, see paper 1, the two minima become similar in depth when spin−orbit coupling is included. The mechanism by which spin−orbit coupling has such an important effect on the potentials is explained in Section 4 of paper 1. It is instructive to also compare the lowest spin−orbit adiabatic potential of Br−HCN in Figure 5 of paper 1 with the corresponding adiabatic potential of Cl−HCN in Figure 5, which was computed with exactly the same spin-free potentials but with the much smaller spin−orbit coupling parameter A of Cl. Although for the complex of Br with HCN the two minima in this lowest adiabatic potential are nearly equally deep, the Cl complex gives a minimum for Cl−NCH that is deeper than the Cl−HCN minimum by about 100 cm^{-1}. In addition, the isomerization barrier is much higher for the Cl complex than for the Br complex, nearly 300 cm^{-1} against about 160 cm^{-1}, with respect to the deepest minimum. This is because more of the spin-free state P_0 (with the deep minimum in $V_{0,0}$) remains in the lowest spin−orbit adiabatic state for Cl−HCN than for Br−HCN because the spin−orbit coupling is less-dominant.

Another effect of the smaller spin−orbit coupling is that the ground-state parity splitting calculated for Cl−NCH is not $4B$ as in Br−NCH, but about $3B$. According to the explanation of the parity splittings in Section 3.2, this implies that the effective electronic angular momentum, j_A, for ground-state Cl−NCH is smaller than the value for the Br−NCH complex, which was close to the atomic value of $(^3/_2)$. So, one observes that most of the difference of 157 cm^{-1} in D_0 between Cl−NCH and Cl−HCN can be understood from the difference in the well depths in the lowest spin−orbit adiabatic state. The remainder must be a dynamical effect, related to the fact that the nuclear motion problem must be solved with multiple coupled potential surfaces, not just on the lowest adiabatic potential.

6. Conclusions

In the preceding paper (paper 1), we presented the full 3×3 matrix of diabatic potential surfaces that correlate with the ^2P state of the Br atom. With the use of these potentials and the inclusion of spin−orbit coupling, we computed rovibronic energy levels and properties of the Br(^2P)−HCN complex in full three-dimensional (3D) calculations. Dynamical variables in the 3D model are the distance R between Br and the center of mass of HCN, the CH bond length r_{CH}, and the angle θ between the NCH axis and the Br−HCN axis R. The HCN monomer was kept linear, and the CN bond length was frozen. We also made 2D calculations in which the CH bond length was frozen at the vibrationally averaged values r_0 and r_1 and 2+1D calculations in which the 3D potentials were averaged over the $v = 0$ and $v = 1$ vibrational wave functions of the CH stretch mode in HCN. Furthermore, we performed 2D calculations for r_{CH} frozen at the HCN equilibrium value r_e and 1D calculations in which both r_{CH} and the Br−HCN distance R were frozen.

The complex is found to have two linear structures with nearly equal binding energies, Br−NCH and Br−HCN. The calculated binding energies are $D_0 = 352.4$ cm^{-1} and $D_0 = 349.1$ cm^{-1}, respectively. Both isomers were found experimentally[5] in superfluid helium clusters in a molecular beam setup. From the infrared spectra associated with the CH stretch mode in both isomers, it was concluded that Br−NCH has a ground state with $J = |\Omega| = (^1/_2)$ and that Br−HCN has a ground state with $J = |\Omega| = (^3/_2)$. This is what we found in our calculations as well. It could be understood on the basis of the adiabatic and diabatic potential energy surfaces of paper 1, which are qualitatively determined by the electrostatic interaction between the quadrupole of the Br(^2P) atom and the dipole of HCN, and the very strong spin−orbit coupling in Br. We predicted the frequencies of the van der Waals modes of both isomers, both for $v = 0$ and $v = 1$ of the CH stretch mode of HCN, and extracted a set of spectroscopic constants from the energy levels calculated for $J = (^1/_2)$ to $(^7/_2)$. For Br−HCN with its degenerate spin-free ground state of Π symmetry the bend fundamental with $v_b = 1$ and vibrational angular momentum $\omega_B = \pm 1$, interacting with the electronic $^2\Pi$ state with $\mu = \pm 1$, produces levels with $|\Omega| = (^1/_2)$ and $|\Omega| = (^5/_2)$ that are split by 2.6 cm^{-1}, a Renner−Teller nonadiabatic coupling effect. For Br−NCH with its nondegenerate Σ ground state, there is a small indirect Renner−Teller splitting of 0.9 cm^{-1} caused by spin−orbit coupling-induced $\Sigma−\Pi$ mixing. The red shift of the CH stretch frequency in the complex, relative to free HCN, was calculated to be 1.98 cm^{-1} for Br−NCH and 23.11 cm^{-1} for Br−HCN. The experimental[5] values, corrected for the helium matrix shift, are 1.65 and 23.80 cm^{-1}.

Another property that could be compared with experiment is the splitting of the rovibronic levels of e and f spectroscopic parity. Relatively large first-order parity splittings were calculated and theoretically explained for the levels of Br−NCH with bend vibration angular momentum $\omega_B = 0$. All other levels of Br−NCH and the levels of Br−HCN have splittings that are smaller by several orders of magnitude. The large splitting was indeed observed in the experimental spectrum of Br−NCH,[5] but it was smaller than predicted. We believe this to be an effect of the surrounding helium cluster, which is known to also reduce the rotational constants by a factor of nearly 3. When we compared the calculated and measured rotational constants B, such a reduction was indeed found, for both Br−NCH and Br−HCN. The reduction of the parity splitting is larger by another factor of 2, however.

Finally, we found an explanation why for the corresponding Cl complex only the linear Cl−NCH isomer was observed, not the Cl−HCN isomer. We made model calculations with the potential energy surfaces computed for the Br complex in paper 1, but with the spin−orbit coupling constant $A = 882.4$ cm^{-1} of Cl instead of $A = 3685.5$ cm^{-1} for Br. The hydrogen-bonded isomer Cl−HCN turned out to be less-stable than Cl−NCH by nearly 160 cm^{-1}, whereas Br−HCN is less stable than Br−NCH by only 3.3 cm^{-1}. A large part of this energy difference could be understood by a comparison of the lowest spin−orbit adiabatic potential surfaces of the Br and Cl complexes. In addition, the isomerization barrier is much higher for the Cl complex than for the Br complex. The same set of spin-free adiabatic and diabatic potentials gives remarkably different adiabatic potential surfaces when a different spin−orbit coupling term is included.

References and Notes

(1) Andrews, L.; Hunt, R. D. *J. Chem. Phys.* **1988**, *89*, 3502.

(2) Bradforth, S. E.; Weaver, A.; Arnold, D. W.; Metz, R. B.; Neumark, D. M. *J. Chem. Phys.* **1990**, *92*, 7205.

(3) Liu, K.; Kolessov, A.; Partin, J. W.; Bezel, I.; Wittig, C. *Chem. Phys. Lett.* **1999**, *299*, 374.

(4) Merritt, J. M.; Küpper, J.; Miller, R. E. *Phys. Chem. Chem. Phys.* **2005**, *7*, 67.

(5) Merritt, J. M.; Küpper, J.; Miller, R. E. *Phys. Chem. Chem. Phys.* **2007**, *9*, 401.

(6) Meuwly, M.; Hutson, J. M. *J. Chem. Phys.* **2000**, *112*, 592.

(7) Meuwly, M.; Hutson, J. M. *J. Chem. Phys.* **2003**, *119*, 8873.

(8) Žďánska, P.; Nachtigallová, D.; Nachtigall, P.; Jungwirth, P. *J. Chem. Phys.* **2001**, *115*, 5974.

(9) Kłos, J.; Szczęśniak, M. M.; Chałasiński, G. *Int. Rev. Phys. Chem.* **2004**, *23*, 541.

(10) Zeimen, W. B.; Kłos, J. A.; Groenenboom, G. C.; van der Avoird, A. *J. Phys. Chem. A* **2003**, *107*, 5110.

(11) Zeimen, W. B.; Kłos, J.; Groenenboom, G. C.; van der Avoird, A. *J. Phys. Chem. A* **2004**, *108*, 9319.

(12) Fishchuk, A. V.; Wormer, P. E. S.; van der Avoird, A. *J. Phys. Chem. A* **2006**, *110*, 5273.

(13) Fishchuk, A. V.; Groenenboom, G. C.; van der Avoird, A. *J. Phys. Chem. A* **2006**, *110*, 5280.

(14) Zeimen, W. B.; Kłos, J. A.; Groenenboom, G. C.; van der Avoird, A. *J. Chem. Phys.* **2003**, *118*, 7340.

(15) Alexander, M. H. *J. Chem. Phys.* **1993**, *99*, 6014.

(16) Dubernet, M.-L.; Hutson, J. M. *J. Chem. Phys.* **1994**, *101*, 1939.

(17) Dubernet, M.-L.; Hutson, J. M. *J. Phys. Chem.* **1994**, *98*, 5844.

(18) *Handbook of Chemistry and Physics*; Lide, D. R., Frederikse, H. P. R., Eds.; Chemical Rubber: Boca Raton, FL, 1997.

(19) Carter, S.; Mills, I. M.; Handy, N. C. *J. Chem. Phys.* **1990**, *99*, 4379.

(20) Metz, R. B.; Pfeiffer, J. M.; Thoemke, J. D.; Crim, F. F. *Chem. Phys. Lett.* **1994**, *221*, 347.

(21) Sims, I. R.; Smith, I. W. M. *J. Chem. Soc., Faraday Trans. 2* **1989**, *85*, 915.

(22) Frost, M. J.; Smith, I. W. M.; Spencer-Smith, R. D. *J. Chem. Soc., Faraday Trans. 2* **1993**, *89*, 2355.

(23) Groenenboom, G. C.; Colbert, D. T. *J. Chem. Phys.* **1993**, *99*, 9681.

2. Bound-State Calculations and Infrared Spectra

J. Phys. Chem. A, Vol. 111, No. 31, 2007 **7281**

(24) Holmgren, S. L.; Waldman, M.; Klemperer, W. *J. Chem. Phys.* **1977**, *67*, 4414.

(25) Alexander, M. H.; Gregurick, S.; Dagdigian, P. *J. Chem. Phys.* **1994**, *101*, 2887.

(26) Herzberg, G. *Molecular Spectra and Molecular Structure, Vol. 3: Electronic Spectra and Electronic Structure of Polyatomic Molecules*; Van Nostrand: New York, 1950.

(27) Lefebvre-Brion, H.; Field, R. W. *Perturbations in the Spectra of Diatomic Molecules;* Academic: New York, 1986.

(28) Renner, R. *Z. Phys.* **1934**, *92*, 172. English translation in Hettema, H. *Quantum Chemistry: Classic Scientific Papers*; World Scientific: Singapore, 2000.

(29) Pople, J. A.; Longuet-Higgins, H. C. *Mol. Phys.* **1958**, *1*, 372.

(30) Dhont, G.; Zeimen, W. B.; Groenenboom, G. C.; van der Avoird, A. *J. Chem. Phys.* **2004**, *120*, 103.

(31) Choi, M. Y.; Douberly, G. E.; Falconer, T. M.; Lewis, W. K.; Lindsay, C. M.; Merritt, J. M.; Stiles, P. L.; Miller, R. E. *Int. Rev. Phys. Chem.* **2006**, *25*, 15.